Kovove Mater. 59 2021 345–355
DOI: 10.4149/km_2021_6_345

Effect of aging heat treatment on mechanical properties of expanded glass reinforced syntactic metal foam

İ. C. Akgün*, Ç. Bolat, A. Gökşenli

Faculty of Mechanical Engineering, Istanbul Technical University, 34437 Istanbul, Turkey

Received 7 June 2021, received in revised form 12 October 2021, accepted 13 October 2021

Abstract

Metal matrix syntactic foams (MMSFs) are advanced engineering materials, and their properties like low density, high compression strength, good ductility, and excellent energy absorption capability make them considerably attractive for many industrial applications nowadays. In this research paper, a new production method named sandwich infiltration casting was used to manufacture metal syntactic foams, including Al 7075 matrix and expanded glass (EG) fillers with 2–4 mm diameter. As a result of the porous structure of EG particles, density values of the fabricated aluminum matrix syntactic foams (AMSFs) changed between 1.39 and 1.47 g cm^{-3}. Micro observations showed that there was perfect harmony between the matrix and EG particles as a consequence of effective process optimization and adequate wettability of the EG spheres. In addition, T6 heat treatment was applied to specific samples to analyze the possible effect of aging on the mechanical properties. The results indicated that expanded glass had great potential for syntactic foam applications compared to the other filler types utilized in previous efforts. Moreover, it was apparent that there was a favorable relationship between the heat treatment and compressive properties (compression strength, plateau strength, and energy absorption ability) of the fabricated foams.

K e y w o r d s: metal syntactic foams, compression strength, energy absorption ability, expanded glass fillers

1. Introduction

Metallic foams are advanced engineering materials consisting of a metal matrix containing inner pores. They have become popular nowadays due to their exceptional compressive properties, low density, decent strength to weight ratio, high stiffness, and remarkable energy absorption ability [1–5]. Metal matrix syntactic foams (MMSFs) are a subgroup of metallic foams that uses a filler granule to constitute porosity. MMSFs have outstanding mechanical properties compared to traditional metal foams [6–14]. The main advantage of MMSFs is the control of porosity size and shape, resulting in a narrow density variation which is very important in the future for serial production. MMSFs have become popular for several industrial areas such as automotive [15, 16], aerospace [17], construction [18], shipbuilding [19], railway [20], and biomedical applications [9, 21]. As matrix material, different metallic materials such as aluminum [22], steel [23], titanium [24], magnesium [25], etc. are used. As filler material, hollow ceramic spheres [8], micro-glass balloons [9], fly ash cenospheres [10], and hollow metal spheres are used [26]. The sizes of the spheres change from 0.01 to 10 mm.

Different fabrication methods have been developed to produce MMSFs. The powder metallurgical method is promising, but the risk of sphere fracture still exists. By the stir casting method, hollow spheres are mixed inside liquid metal and stirred. Despite its low cost and easy application, the main disadvantages of this method are that by mechanical mixing process, sphere fraction may occur, and an inhomogeneous structure due to density variation may form. The pressure infiltration method is the most preferred method for MMSFs production due to the homogeneous and controllable inner structure. Infiltration method can be classified as gravity-assisted [27, 28], counter grav-

*Corresponding author: e-mail address: akgunism@itu.edu.tr

ity [29], gas/vacuum-assisted [30, 31] and mechanical infiltration [32, 33] methods. In the mechanical infiltration method, casting pressure is constituted by a piston resulting in higher pressure values completion in the fabrication of complex geometries [34–36]. In our study, we developed a novel production technique called sandwich infiltration casting, which puts gravity-assisted and counter gravity melt infiltration techniques together to form a uniform matrix/filler structure along with the accurate part geometry.

In recent years, aluminum has been frequently preferred as matrix metal by MMSFs production due to its low density and widespread usage in several industries. Many different Al series are utilized with different types of filler particles to determine mechanical features and understand deformation/fracture mechanisms exhaustively [37–39]. Mondal et al. [40] compared alumina and cenosphere-reinforced Al syntactic and reported that although cenosphere filled samples showed higher energy absorption capacity under compressive loading, alumina filled foams had better matrix/filler bonding ability. To determine the tribological behavior of aluminum matrix syntactic foams (AMSFs), Chaitanya et al. [41] studied the wear performance of cenosphere-reinforced Al syntactic by applying a pin-on-disc test and pointed out that the wear rate diminished with increasing sliding speed. In another research, contrary to widely performed experimental works, Chordiya et al. [42] simulated the low-speed impact behavior of Al syntactic making use of a free-fall drop impact testing system, so they modeled different impact speeds and sample models. Apart from these newest researches, some researchers worked on heat treating AMSFs and studied Al alloys as matrix materials due to their large-scale usage in several industrial applications and applicability for heat treatment procedures for matrix strengthening. At this point, Rao et al. [43] applied different heat treatments on Al_2O_3 7055-Al matrix syntactic foam samples and reported that the heat treatment improved plateau strength and absorbed energy of the fabricated syntactic. Movahedi et al. [29] investigated the probable effects of the heat treatment on expanded perlite filled Zinc (ZA27) syntactic foam and found that applied heat treatment enhanced the specific energy absorption, plateau stress, and energy absorption efficiency of produced foams. Similar improvements in the compression features were observed for T6 treated ceramic microspheres (45 vol.% $3Al_2O_3$-$2SiO_2$ and 55 vol.% SiO_2) reinforced Al 7075 syntactic foam by Dunand et al. [30]. In another effort, Santa Maria et al. [31] tried to understand the effects of T4 and T7 treatment on the deformation behavior of Al 206/Al_2O_3 syntactic foam, and the research team indicated that heat-treated samples had better average peak strength and specific plateau strength values than their as-cast versions.

From the formerly published efforts [7, 12, 14, 30, 44], various types of deformation behavior are possible for MMSFs according to matrix metal type, filler material, harmony between the constituents, production method, and presence of heat treatment. As long as the matrix strength exceeds the crush strength of the filler particles, the primary deformation mechanism reflects ductile characteristics; however, when the filler crush strength is higher than the matrix flow strength, usually brittle deformation is the predominant mechanism. Apart from that, sometimes, on account of heterogeneous pore structure and distribution of the filler particles, the mixed mechanism (ductile + brittle) is effective on the characteristic of the foam deformation.

In this research, 7075 series of aluminum alloy was chosen as matrix metal, and as reinforcement material, expanded glass (EG) was selected due to its extremely porous structure and low cost. As for the production method, the novel technique called sandwich infiltration casting was used. Later on, we applied T6 heat treatment to some of the fabricated AMSFs. Furthermore, macro/micro investigations and quasi-static compression tests were conducted to analyze the mechanical properties of the AMSFs.

The principal aim of this investigation was to examine the effect of applying T6 treatment on the mechanical properties and fracture mechanisms of AMSFs produced by a novel developed sandwich casting method.

2. Methods and materials

As a well-known member of 7000 series of Al alloys, 7075 was used in this investigation as matrix metal due to its widespread usage in many sectors and outstanding potential for the T6 heat-treatment process. The Al blocks were supplied from Güray Aluminum Limited Company – Turkey. According to supplier information, the matrix alloy comprises 5.68 wt.% Zn, 2.39 wt.% Mg, 1.4 wt.% Cu, 0.21 wt.% Fe, 0.2 wt.% Si, 0.18 wt.% Mn, 0.034 wt.% Ti, and 0.018 wt.% Zr. As for filler material, 2–4 mm Stikloporas® Expanded Glass (EG) spheres were used, and all of them were procured from Omnis Composite Limited Company – Turkey. The supplier stated that the chemical composition of the spheres was 71–73 wt.% SiO_2, 13–14 wt.% Na_2O + K_2O, 8.5–10.5 wt.% CaO + MgO, and other oxides. EG particles, obtained by recycling the scrap glass into a small cellular/porous structure with a special patented technology, are special thermal insulation materials. Due to its low bulk density (0.2 g cm^{-3}), low heat conduction coefficient (0.064 W m^{-1}K^{-1}), and especially low manufacturing costs, EG can be an attractive alternative space holder in syntactic foam compared with engineered hollow

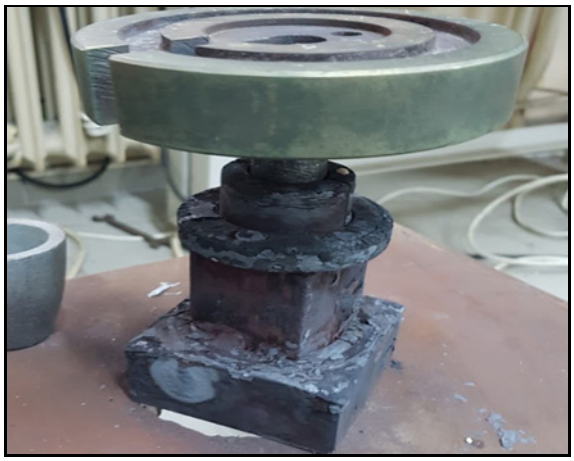

Fig. 1. The mold used in AMSFs production.

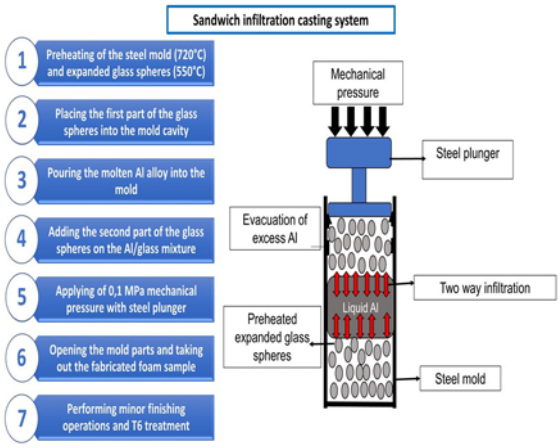

Fig. 2. Sandwich infiltration casting method.

ceramic fillers. Besides, softening temperature of EG spheres is 700 ℃.

Due to manufacturing processes and/or transportation, EG particles may have contained crumbles and glass dust. Before the casting operation, EG particles were filtered with a proper strainer, and the particle size range was kept constant between 2–4 mm.

2.1. Production of AMSF samples

A new manufacturing approach called "sandwich infiltration casting" was used to produce AMSFs. The method aims to have flawless complete infiltration and form a homogeneous foam structure with minimum effort and equipment differently from the other techniques in which steel meshes, vacuum systems, and sophisticated mold parts are utilized. At the first stage, the steel mold is heated up in a 550 ℃ furnace for one hour, then taken out, and 3 g of EG was placed inside the mold. Next, the EG particles were preheated to 550 ℃ to prevent early solidification of molten Al during the infiltration phase. Further, the molten Al, which is freed from dross, was poured into the mold up to 3/4 height of the cavity, and later 2 g of EG was placed on aluminum. Immediately after, a pin-disc element was placed on the mold cavity with a weight of 1 kg to constitute a casting pressure of 25 kPa. A tight gap was between the pin and mold cavity to permit relative motion. Next, the mold and foam samples were cooled down to room temperature in the air. Finally, the mold was carefully opened, and the sample was ejected manually. Figure 1 indicates the mold, Fig. 2 demonstrates the process steps and schematic view of the fabrication of AMSFs.

The fabricated samples can be seen in Fig. 3. The height of the cylindrical sample was 31 ± 0.7 mm and diameter 25 ± 0.1 mm. Before the mechanical tests, all imperfections were cleaned, ground, and polished sensitively.

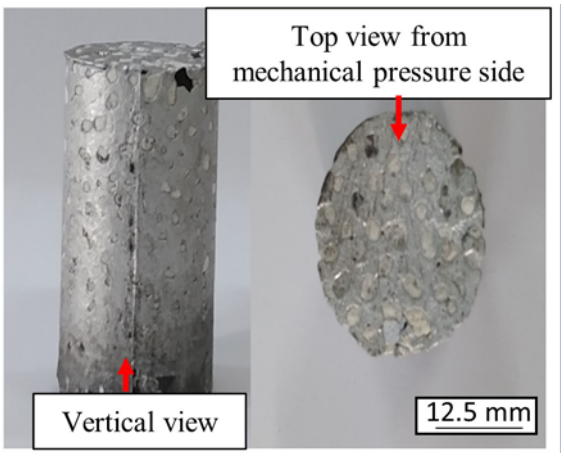

Fig. 3. Cylindrical foam sample.

To analyze the effect of heat treatment on the mechanical properties and fracture mechanism, T6 heat treatment was performed on some selected specimens. An increase of strength was expected after T6 heat treatment due to precipitation of finely dispersed η and η^{I} precipitates both within grains and along grain boundaries [45]. At the first stage, samples were heated to 480 ℃, held for two hours, followed by water quenching. Then, the aging process was carried out at 120 ℃ for 24 h. Applied T6 operation is summarized in Fig. 4.

2.2. Sample characterization

For the microstructural analysis of the expanded glass spheres and syntactic foams samples, scanning electron microscopy (SEM), Nikon Eclipse LV150L, and Nikon SMZ800 model optical microscopes with DpxView-Pro software were used for detailed obser-

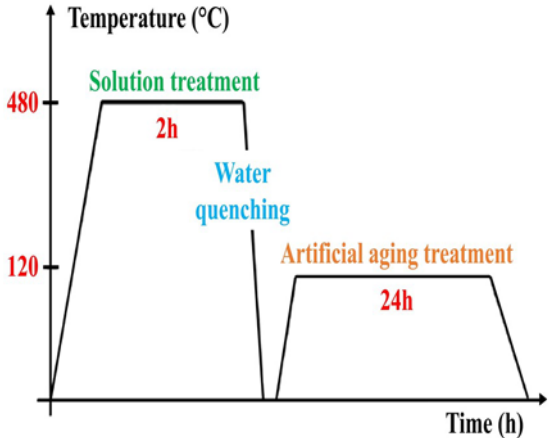

Fig. 4. Applied T6 heat-treatment process.

vations. For microscopic observations, samples were cut and subjected to grinding process using 180-1000 grit with SiC emery papers in Metcon Forcipol 2V machine before polishing which was implemented by utilizing 1 µm Metkon Diapat diamond suspension. Further, polished samples were cleaned in an ultrasonic bath to remove micronized contaminations or unwanted accumulations.

As for physical characterization, the density of the syntactic foam samples (ϕ_{SF}) was calculated by using the Eq. (1):

$$\phi_{SF} = \frac{m_{SF}}{V_{SF}}, \tag{1}$$

where V_{SF} is the volume of the sample and m_{SF} is the mass of the sample. The mass of the samples was measured by using a precision scale with an accuracy of ± 0.0001 g.

To determine the volume fraction of filler particles (F_{Fil}) and total porosity percentage (F_{TP}), mathematical equations expressed by Taherishargh [44] were used. In these equations, (Eqs. (2)–(4)), V_{syn}, m_{syn}, m_{fil}, ρ_{fil}, ρ_{alu}, and ρ_{sd} are the syntactic foam volume, the foam mass, the mass of EG spheres, particle density of EG, the density of the matrix, and density of solid-state of the EG spheres, respectively:

$$F_{Fil} = \left[V_{syn} - \left(\frac{m_{syn} - m_{fil}}{\rho_{alu}}\right)\frac{1}{V_{syn}}\right] \times 100, \tag{2}$$

$$\rho_{fil} = \frac{m_{fil}}{V_{syn} - \left(\dfrac{m_{syn} - m_{fil}}{\rho_{alu}}\right)}, \tag{3}$$

$$F_{TP} = F_{Fil}\left[1 - \rho_{fil}/\rho_{sd}\right]. \tag{4}$$

Mechanical properties of the samples were determined using compression tests through a computer-controlled 50 kN Shimadzu AG-IS uniaxial testing machine cooperating with Trapezium 2 data acquisition software. The load and displacement data were collected throughout the compression and converted to engineering stress-strain curves using initial sample height and cross-sectional area. The deformation rate was kept constant as 1 mm min^{-1} during the test. A lubricant was rubbed on related surfaces of compression platens immediately before the tests to apply uniform uniaxial loading and prevent barreling. In addition, we recorded all tests via a digital camera to understand the failure mechanism of the foams better.

To determine mechanical properties, compression strength (1 % proof strength), plateau stress, plateau end strain, densification strain energy absorption, and energy absorption efficiency values were calculated using the stress-strain curves in conformity to ISO 13314 [46]. Initially, in the elastic zone, the slope of the linear section was used to decide compression strength. Following the linear section, stress values go down depending on sample properties (matrix strength, filler strength, particle diameter, porosity style), and the plateau zone starts up. As for plateau stress, the arithmetic mean of the stress values between 0.2 and 0.4 strain was calculated using data collected via Trapezium 2 software. Plateau end strain value is the strain value at which the stress is 1.3 times the plateau stress. As energy absorption values (W) were appointed, recorded data from the stress-strain curve was integrated up to 0.5 strain. Lastly, the energy absorption efficiency (η) was calculated by using Eq. (6), where σ_{max} is the maximum compressive stress up to 50 % strain:

$$W = \int_0^{0.5} \sigma \mathrm{d}\varepsilon, \tag{5}$$

$$\eta = \frac{W}{0.5\sigma_{max}}. \tag{6}$$

3. Results and discussion

3.1. Microstructural analysis of EG spheres and produced syntactic foams

It can be seen from the macroscopic views in Fig. 5 that the spheres are spherical and closed structures. Also, the inner porous structure can be seen. In addition, Fig. 6 shows detailed SEM views of the inner porous structure and the outer surface of the EG spheres. This structure consists of closed cells and struts. A similar observation was also detected by Su et al. [20].

The typical microstructure of the manufactured foams is represented in Fig. 7, and it reflects very similar features as described for the MMSFs [11]. Figure 7 demonstrates that all samples have perfect infiltration

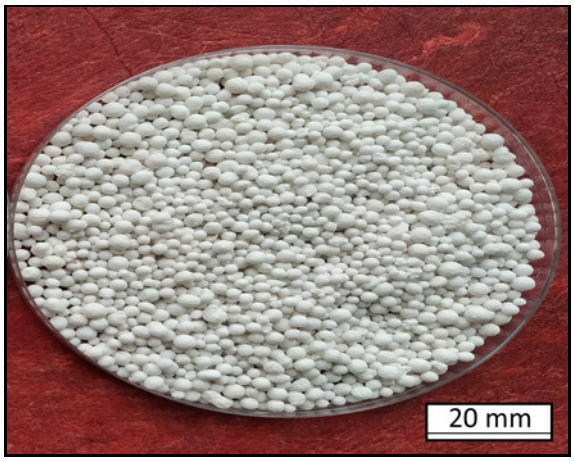

Fig. 5. Macro photograph of expanded glass granules.

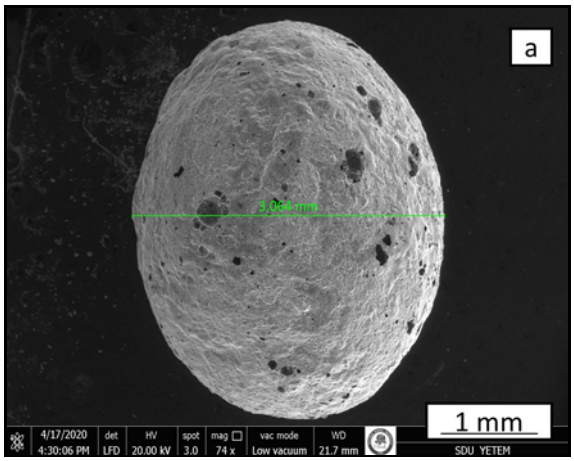

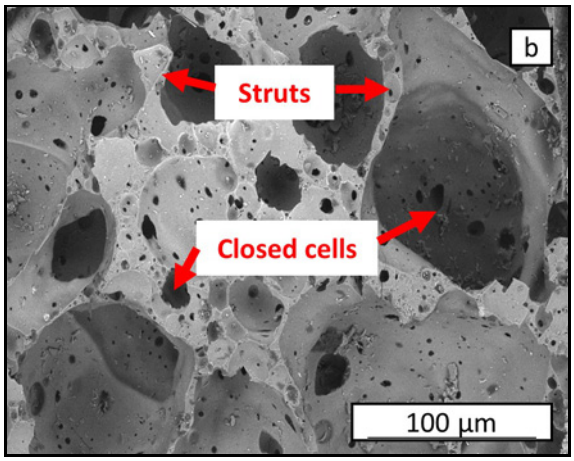

Fig. 6. SEM images of expanded glass particle (a) and inner porous structure (b).

harmony due to the superior infiltration ability of the sandwich infiltration casting offered by our research team and the good wettability of the expanded glass (EG) spheres. Moreover, we observed successful infiltration processes between EG particles even in quite

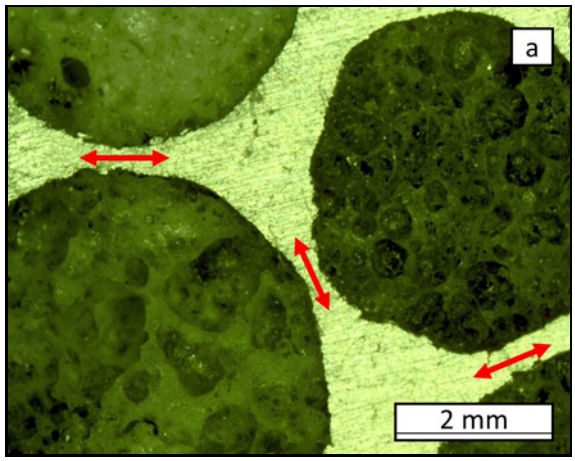

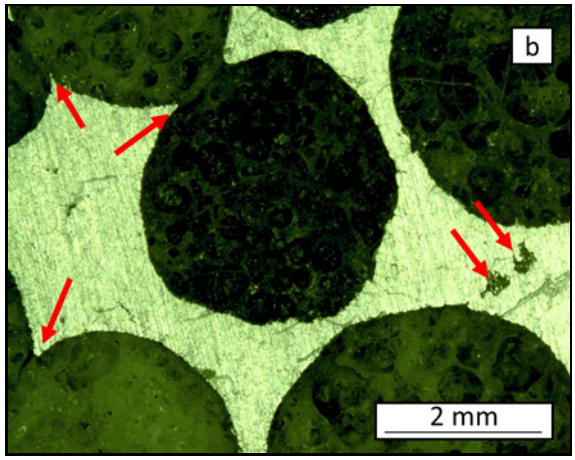

Fig. 7. Microscopic views of produced samples: infiltration between narrow gaps (a) and casting voids (b).

narrow gaps at the optimum production parameters. Throughout the production process, it can be considered that certain filler particles tending to merge are indicated by black arrows in Fig. 7a. Indeed, this can be seen as partial sintering and observed locally in all foam samples; thus, it can be asserted that infiltration temperature and process pressure are substantially responsible for the diffusion of the surface atoms of the EG spheres. Aside from that, some minor negligible casting voids resulting from matrix shrinkage in the solidification stage were noticed, as shown in Fig. 7b. Herein, it can be estimated that this kind of cavities might form around the matrix/filler interface during solidification because of the different thermal conductivity of the EG particles and the matrix alloy, and they might also occur in the matrix itself infrequently. However, no infiltration of the aluminum inside the spheres was detected.

3.2. Physical properties of produced AMSFs

The volume fraction of filler particles (F_{Fil}) and total porosity percentage (F_{TP}) were determined by

Table 1. Physical properties of produced AMSFs

Sample	Height (mm)	Diameter (mm)	Density ($g\,cm^{-3}$)	Filler volume (%)	Total porosity (%)
SF1	30.79	25.03	1.39	62.3	49.7
SF2	30.73	24.94	1.46	59.9	47.2
SF3	31.21	25.09	1.42	61.0	48.5
SF4-T6	31.58	24.98	1.47	59.2	46.9
SF5-T6	30.35	25.02	1.42	61.4	48.6
SF6-T6	31.09	25.06	1.40	61.8	49.3

using Eqs. (2)–(4). The results can be seen in Table 1.

According to physical analysis, the average density value of all samples is $1.42\,g\,cm^{-3}$, while the lowest is $1.39\,g\,cm^{-3}$ for SF1. These values are compatible with previous literature efforts and can be considered a low-density category compared to other foams fabricated in technical literature [47–49]. Since the volume-controlled design of the sandwich infiltration casting allows the porous EG spheres to fill the mold cavity effectively by assembling the top and bottom sections, it plays an important role in total density drop. EG particles are substantially hard and stiff materials and have many small pores in their solid bodies. In addition, they are resistant against either crushing under fabrication pressure or liquid matrix metal leakage into the inner rooms, thanks to their strong and smooth surface structure. Indeed, both damaged fillers and matrix leakage can be evaluated as undesired circumstances because they cause density increase and can dominate the fractured style of the AMSFs. Herein, compared to the EG, some engineered hollow fillers used in technical literature like special ceramic mixtures and microspheres are more sensitive to cracking and molten matrix penetration [12, 34, 36]. The porosity of the produced AMSFs was calculated using Eq. (2)–(4). Porosity values of the AMSFs remain between a narrow band from 46.9–49.7 %. Applying heat treatment T6 did not affect the density and porosity of the AMSFs samples.

3.3. Compressive properties of the produced AMSFs

All fabricated specimens were prepared for compression tests, and T6 heat treatment was applied to three of them. The compressive stress-strain curves of as-cast and T6 heat-treated AMSFs samples can be seen in Figs. 8 and 9, respectively. All curves show typical stress-strain curves. A linear deformation occurs at low strain values. After a stress peak, the stress value decreases slightly, and a typical plateau region starts while the stress value fluctuates slightly or remains constant plateau stress; meanwhile, continuous plastic deformation occurs. This characteristic is very important for syntactic foam metals when high energy absorption is desired. Most of the space holder (EG spheres) collapses in the final stage, and the stress value increases suddenly.

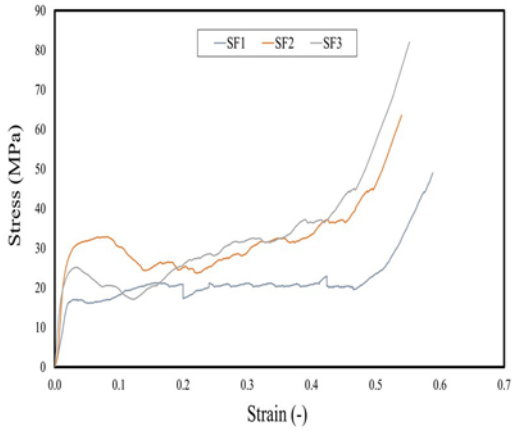

Fig. 8. Compressive stress-strain curves of as-cast produced syntactic foams depending on different average density values.

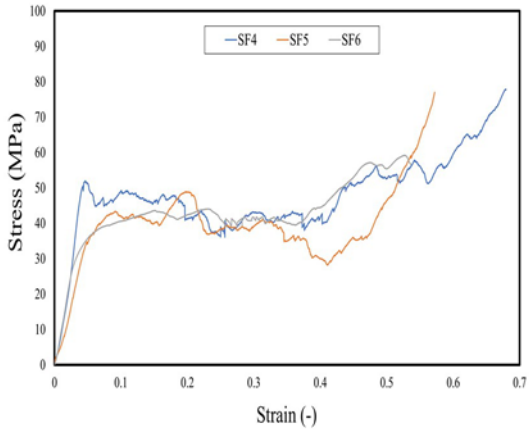

Fig. 9. Compressive stress-strain curves of T6 heat treated syntactic foams depending on different average density values.

Table 2 summarizes the compressive test results. σ_{cmp}, σ_{pl}, ε_{dsf}, W, and η are compression strength,

Table 2. Main compressive properties of produced AMSFs

Foam No.	σ_{cmp} (MPa)	σ_{pl} (MPa)	ε_{dsf} (–)	W (MJ m^{-3})	η (–)
SF1	15.9	20.3	0.52	9.7	0.90
SF2	28.8	29.0	0.45	15.0	0.82
SF3	23.6	31.3	0.44	14.7	0.81
SF4-T6	49.8	40.9	0.56	21.5	0.79
SF5-T6	39.1	38.2	0.51	18.3	0.76
SF6-T6	35.1	41.6	0.47	20.8	0.92

plateau stress, plateau end strain value, energy absorption, and energy absorption efficiency values, respectively.

As known from the literature [50], solid as-cast Al alloys have lower yield strength than the T6 heat-treated alloys. This circumstance is also observed in the syntactic foam structures because the Al matrix supports most of the compressive load during deformation. Compression strength values of heat-treated syntactic foams exceed the corresponding value for as-cast foam at near density values for all samples. The filler materials are weaker to contribute to the compression strength of the foams. Average compression proof strength values of as-cast and heat-treated foams are 22.8 and 41.3 MPa, respectively. The plateau stress (σ_{pl}) is another property of AMSFs that plays an important role for endurance to deformation during large-strain compression and for the ability of energy absorption. In a similar vein to the compressive strength, the plateau stress values of heat-treated samples are quite higher than as-cast foams. Heat-treated foams have higher plateau stress values than the as-cast samples with an average value of 40.2 MPa, while the average plateau stress value of as-cast foams is 26.9 MPa. Heat-treated syntactic foam samples show a detectably higher performance in terms of energy absorption ability compared to as-cast foams. This improvement can be explained by high compressive response stress levels of heat-treated samples despite ductility decrease in the matrix. The highest energy absorption value is 21.5 MJ m^{-3} for heat treated and 15 MJ m^{-3} for as-cast samples. On the other hand, no distinct effect of heat treatment on plateau end strain value was determined; the average densification strain value of 0.51 was read for T6 treated foams and 0.47 for as-cast foams. Afterward, the effect of produced syntactic foam specimen density on mechanical properties was investigated, as shown in Fig. 10.

There is a general assumption that mechanical features of MMSFs improve with their increasing density values but sometimes, small differences may be noticed between almost the same or close density foams. Therefore, a possible explanation is the non-uniform distribution of reinforcements in the matrix material (random filling/packing) along with the non-uniform size and shape of the filler particles. Addi-

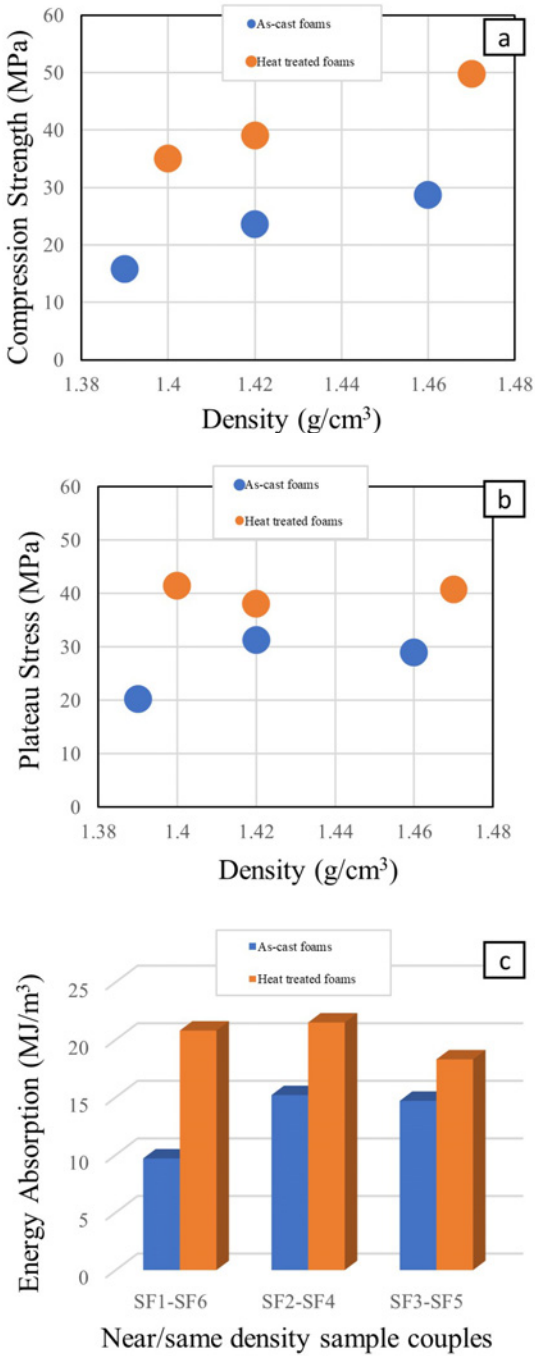

Fig. 10. Binary comparison between density and mechanical properties: compressive strength (a), plateau stress (b), and energy absorption (c).

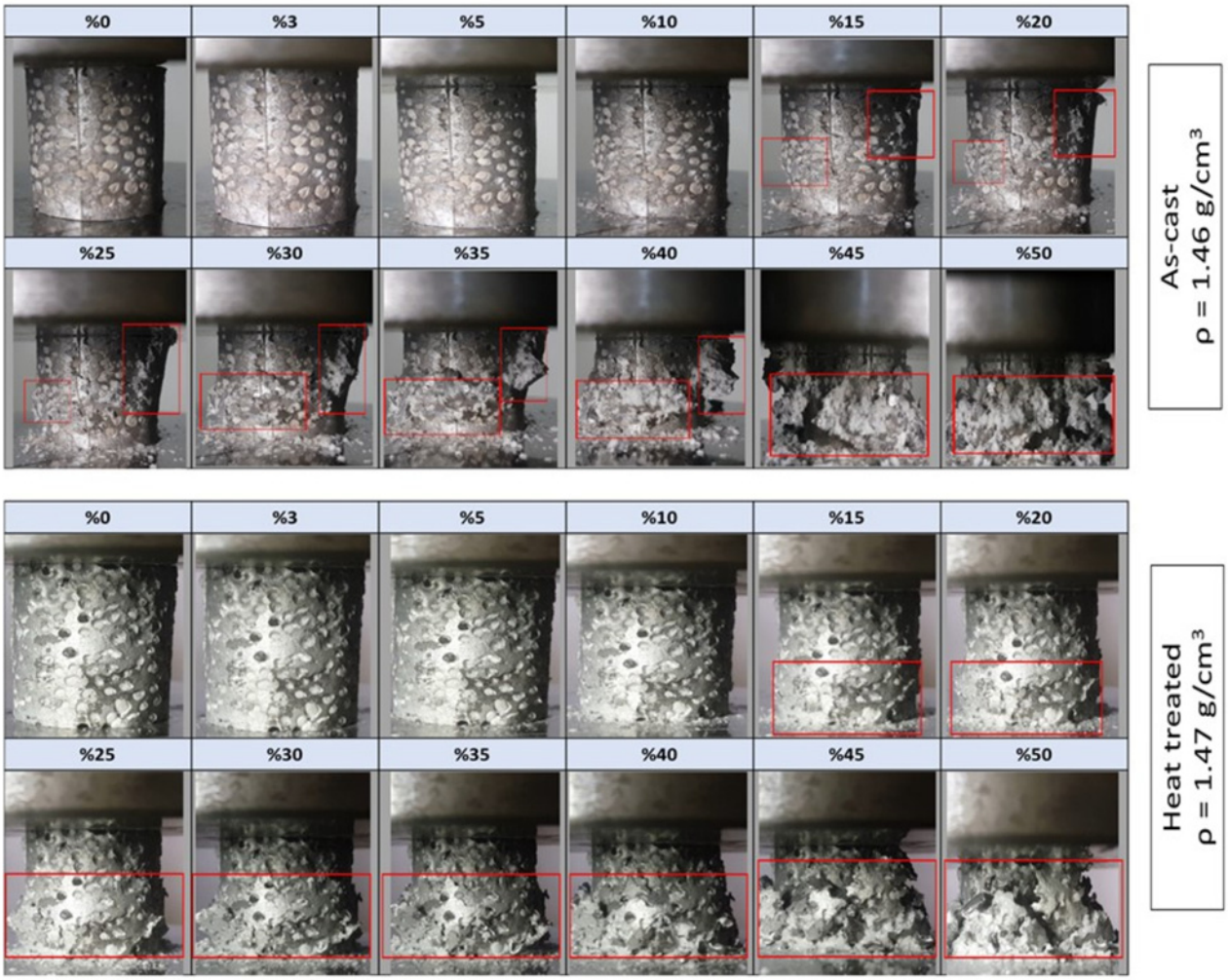

Fig. 11. Deformation behavior of the foam samples.

tionally, mechanical anisotropy due to the irregular porous structure of filler materials may be observed in some cases. From Fig. 10a, it can be stated that there is a positive effect of density rising on the compressive strength of the foams since higher density corresponds to higher matrix volume fraction in the syntactic structure. However, no explicit relation was determined between density and plateau stress value in both as-plated and heat-treated samples. From the experimental results, the energy absorption efficiency of syntactic samples is not related to the foam density, and it is an independent parameter, just as other researchers considered before [30, 51]. The energy efficiency of the samples varies between 0.76 and 0.92, and it depends hugely on ideal flat behavior in the plateau zone. In addition, there is no relationship between the energy absorption efficiency and heat treatment for all samples. Principle mechanisms affecting the efficiency are filler properties like size, pore style, and shape rather than the heat treatment. Even though heat-treated sample SF6 has the highest efficiency with 0.92, the average of all types of foams is 0.83.

3.4. Failure mechanisms

Figure 11 demonstrates images taken during the deformation of EG-filled foam samples with increasing strain rates. As-cast foam initially behaves elastically, but it starts to deform in a ductile manner at 10 % deformation. At 15 % deformation, the barreling effect can be seen clearly on the middle section of the sample body and the other sections, also called death zones, remain undeformed. This situation can be attributed to the existence of a density gradient in the foam body and the porosity volume percentage in middle zones being higher than in the other zones. Additionally, it can be expressed that body sections, including higher porosity, deform earlier due to deformation localization. From Fig. 11, in as-cast samples, between the 20 and 30 % deformation, a new damaged section located in the upper right side of the sample becomes

more apparent due to deformation localization. Beginning from this point of the compression, the failure characteristic of the foam sample can be described as mixed-type deformation. In the mixed-type deformation, ductile and brittle sections with small cracks are present on the sample, and this damage mode is dominant between 40 % and 50 % strain values. Immediately after the compression test, even though deep surface cracks resulting from the sensitivity of crack propagation in the right upper side of the foam body and small discrete body fragments stemming from initial damage of the EG spheres are discerned, it should be emphasized that the foam seems like a one-piece.

The heat-treated foam deforms elastically in the early stages of the mechanical loading, and there is a sharp increment in the stress owing to the elastic deformation of matrix and filler materials. However, its yield strength is higher than that of the as-cast sample due to the dislocation blocking ability of precipitates. Contrary to the as-cast sample, the heat-treated sample displays mixed type deformation in large part of plastic deformation. Between 20–35 % strain, a brittle characteristic can be seen easily due to multiple independent cracks having different lengths and directions. At the same time, a small amount of ductile barreling effect in the bottom sections is also observed. Multiple cracks emerging in the T6 treated sample can be attributed to increased strength and decreasing fracture toughness of the Al matrix. Depending upon continuously formed small cracks, the plateau region has some fluctuations in the heat-treated samples. Similar behavior was also observed by Fiedler et al. [52]. Although perfect infiltration can be created even in very narrow gaps using the sandwich infiltration casting, this fact effectively hinders early crack propagation only for the as-cast sample, not for the T6 treated due to the age hardening. In the as-cast sample, formed cracks grow swiftly in the EG particles, but they are stopped by a ductile matrix. This circumstance is not the same for the T6 treated sample because the Al alloy has low fracture toughness between the brittle EG spheres. Following 40 % deformation, some big-size foam parts separate from the main body due to different rapid crack growths, and when the strain value reaches 50 %, this separation effect maximizes. Compared to its as-cast version, T6 treated sample can't keep its monolithic structure after the compressive load is removed and divides into many discrete parts.

4. Conclusions

As a result of this experimental study focusing on EG filled Al 7075 syntactic foams, some significant-conclusion statements can be emphasized:

1. 2–4 mm EG-filled Al syntactic foams can be produced with the newly introduced sandwich infiltration casting method without extra expensive apparatus or complex-shaped mold designs. Also, since the infiltration stage of the sandwich casting is designed outside of the furnace at room temperature, there is no risk of filler-matrix reaction.

2. Thanks to the sandwich infiltration casting technique, almost 50 % porosity can be attained with a density of 1.39 $\mathrm{g\,cm^{-3}}$ and a filler volume fraction of 62.3 %.

3. T6 heat treatment enhances the compressive properties of the fabricated foams positively. Owing to minimizing dislocation activity in the Al matrix, the compression strength of the T6 treated sample is higher than that of the as-cast samples. Also, as long as the foam densities go up, compression strength values of the samples improve due to the increasing volume fraction of the metallic matrix.

4. Plateau stress values are highly dependent on the heat treatment operation for the produced foams, and the highest value of 41.6 MPa belongs to the T6 treated sample.

5. Maximum and minimum energy absorption values of 21.5 and 18.3 $\mathrm{MJ\,m^{-3}}$ are measured for the T6 treated samples, although the highest value of 15 $\mathrm{MJ\,m^{-3}}$ is observed for produced as-cast samples.

6. Energy absorption efficiency is one of the most important features of the metal syntactic, and it depends substantially on the plateau behavior, so the more the plateau curve is flat, the more efficiency can be obtained. As a result, the term of efficiency is independent of both density and heat treatment.

7. As-cast sample exhibits ductile behavior with the evident barreling effect till the half of the compressive loading, but as the plastic deformation continues, mixed type of deformation becomes apparent.

8. Although the heat-treated sample deforms in a ductile manner at the early stage of the deformation, due to multiple discrete cracks generating on the different zones of the foam body, the brittle fracture mechanism dominates the failure. After the loading, the sample divides into a lot of pieces and loses its one-piece structure ultimately.

Acknowledgements

This article was supported by the Istanbul Technical University – Scientific Research Unit (BAP) with the project ID of MYL-2018-41050. The authors also gratefully thank the Omnis Composite Limited Company for their kind interest in our project and rapid supplying of porous expanded glass spheres.

References

[1] P. Kenesei, C. Kádár, Z. Rajkovits, J. Lendvai, The influence of cell-size distribution on the plastic deformation in metal foams, Scr. Mater. 50 (2004) 295–300. doi:10.1016/j.scriptamat.2003.09.046

[2] U. Ramamurty, A. Paul, Variability in mechanical properties of a metal foam, Acta Mater. 52 (2004) 869–876. doi:10.1016/j.actamat.2003.10.021

[3] E. Linul, D. Pietras, T. Sadowski, L. Marşavina, D. Kumar Rajak, J. Kovacik, Crashworthiness performance of lightweight composite metallic foams at high temperatures, Composites Part A: Applied Science and Manufacturing 149 (2021) 106516. doi:10.1016/j.compositesa.2021.106516

[4] H. X. Zhu, A. H. Windle, Effects of cell irregularity on the high strain compression of open-cell foams, Acta Mater. 50 (2002) 1041–1052. doi:10.1016/S1359-6454(01)00402-5

[5] H. Kiratisaevee, W. J. Cantwell, Low-velocity impact response of high-performance aluminum foam sandwich structures, J. Reinf. Plast. Compos. 24 (2005) 1057–1072. doi:10.1177/0731684405048205

[6] I. N. Orbulov, A. Szlancsik, On the mechanical properties of aluminum matrix syntactic foams, Adv. Eng. Mater. 20 (2018) 1700980. doi:10.1002/adem.201700980

[7] L. Peroni, M. Scapin, M. Avalle, J. Weise, D. Lehmhus, Dynamic mechanical behavior of syntactic iron foams with glass microspheres, Mater. Sci. Eng. A 552 (2012) 364–375. doi:10.1016/j.msea.2012.05.053

[8] P. K. Rohatgi, N. Gupta, B. F. Schultz, D. D. Luong, The synthesis, compressive properties, and applications of metal matrix syntactic foams, JOM 63 (2011) 36–42. doi:10.1007/s11837-011-0026-1

[9] V. Manakari, G. Parande, M. Doddamani, M. Gupta, Evaluation of wear resistance of magnesium/glass micro balloon syntactic foams for engineering/biomedical applications, Ceram. Int. 45 (2019) 9302–9305. doi:10.1016/j.ceramint.2019.01.207

[10] M. D. Goel, V. Parameswaran, D. P. Mondal, High strain rate response of cenosphere-filled aluminum alloy syntactic foam, J. Mater. Eng. Perform. 28 (2019) 4731–4739. doi:10.1007/s11665-019-04237-2

[11] N. Gupta, D. D. Luong, K. Cho, Magnesium matrix composite foams – Density, mechanical properties, and applications, Metals 2 (2012) 238–252. doi:10.3390/met2030238

[12] B. Zhang, Y. Lin, S. Li, D. Zhai, G. Wu, Quasi-static and high strain rates compressive behavior of aluminum matrix syntactic foams, Compos. Part B Eng. 98 (2016) 288–296. doi:10.1016/j.compositesb.2016.05.034

[13] H. Puga, V. H. Carneiro, C. Jesus, J. Pereira, V. Lopes, Influence of particle diameter in mechanical performance of Al expanded clay syntactic foams, Compos. Struct. 184 (2018) 698–703. doi:10.1016/j.compstruct.2017.10.040

[14] A. D. Akinwekomi, J. A. Adebisi, A. A. Adediran, Compressive characteristics of aluminum-fly ash syntactic foams processed by microwave sintering, Metall. Mater. Trans. A Phys. Metall. Mater. Sci. 50 (2019) 4257–4260. doi:10.1007/s11661-019-05347-1

[15] T. D. Claar, C. J. Yu, I. Hall, J. Banhart, J. Baumeister, W. Seeliger, Ultra-lightweight aluminum foam materials for automotive applications, SAE International 724 (2000) Technical paper 2000-01-0335. doi:10.4271/2000-01-0335

[16] V. C. Srivastava, K. L. Sahoo, Processing, stabilization and applications of metallic foams, Art of science, Mater. Sci. Pol. 25 (2007) 733–753.

[17] Z. Nie, Y. Lin, Q. Tong, Numerical simulations of two-phase flow in open-cell metal foams with application to aero-engine separators, Int. J. Heat Mass Transf. 127 (2018) 917–932. doi:10.1016/j.ijheatmasstransfer.2018.08.056

[18] T. Hipke, J. Hohlfeld, S. Rybandt, Functionally aluminum foam composites for building industry, Procedia Mater. Sci. 4 (2014) 133–138. doi:10.1016/j.mspro.2014.07.550

[19] J. Banhart, M. F. Ashby, N. A. Fleck, Metal Foams and Porous Metal Structures. Verlag Metall Innovation Technologie MIT, Bremen, 1999.

[20] M. Su, H. Wang, H. Hao, T. Fiedler, Compressive properties of expanded glass and alumina hollow spheres hybrid reinforced aluminum matrix syntactic foams, J. Alloys Compd. 821 (2020) 153–233. doi:10.1016/j.jallcom.2019.153233

[21] A. Salerno, P. A. Netti, Introduction to Biomedical Foams. Woodhead Publishing Limited, Sawston, 2014.

[22] I. N. Orbulov, Compressive properties of aluminium matrix syntactic foams, Mater. Sci. Eng. A 555 (2012) 52–56. doi:10.1016/j.msea.2012.06.032

[23] Q. Yang, B. Yu, H. Hu, Z. Miao, Y. Wei, W. Sun, Melt flow and solidification during infiltration in making steel matrix syntactic foams, Materials Science and Technology 35 (2019) 1831–1839. doi:10.1080/02670836.2019.1650444

[24] D. P. Mondal, J. D. Majumder, N. Jha, A. Badkul, S. Das, A. Patel, G. Gupta, Titanium-cenosphere syntactic foam made through powder metallurgy route, Materials & Design 34 (2012) 82–89. doi:10.1016/j.matdes.2011.07.055

[25] Q. B. Nguyen, M. L. Sharon, A. S. Nguyen, S. Seetharaman, E. W. Wai, M. Gupta, Synthesis and properties of light weight magnesium-cenosphere composite, Materials Science and Technology 32 (2016) 923–929. doi:10.1080/02670836.2015.1104017

[26] T. J. Lim, B. Smith, D. L. McDowell, Behavior of a random hollow sphere metal foam, Acta Mater. 50 (2002) 2867–2879. doi:10.1016/S1359-6454(02)00111-8

[27] G. Castro, S. R. Nutt, Synthesis of syntactic steel foam using mechanical pressure infiltration, Mater. Sci. Eng. A 535 (2012) 274–280. doi:10.1016/j.msea.2011.12.084

[28] D. W. Huo, J. Yang, X. Y. Zhou, H. Wang, T. K. Zhang, Preparation of open-celled aluminum foams by counter-gravity infiltration casting, Trans. Nonferrous Met. Soc. China (English Ed.) 22 (2012) 85–89. doi:10.1016/S1003-6326(11)61144-8

[29] N. Movahedi, G. E. Murch, I. V. Belova, T. Fiedler, Effect of heat treatment on the compressive behavior of zinc alloy ZA27 syntactic foam, Materials 12 (2019) 792. doi:10.3390/MA12050792

[30] D. K. Balch, J. G. O'Dwyer, G. R. Davis, C. M. Cady, G. T. Gray, D. C. Dunand, Plasticity and damage in aluminum syntactic foams deformed under dynamic and quasi-static conditions, Mater. Sci. Eng. A 391 (2005) 408–417. doi:10.1016/j.msea.2004.09.012

[31] J. A. Santa Maria, B. F. Schultz, J. B. Ferguson, P. K. Rohatgi, Al-Al_2O_3 syntactic foams – Part I: Effect of matrix strength and hollow sphere size on the quasi-static properties of Al-A206/Al2O3 syntactic foams, Mater. Sci. Eng. A 582 (2013) 415–422. doi:10.1016/j.msea.2013.05.081
[32] Y. Lin, Q. Zhang, X. Ma, G. Wu, Mechanical behavior of pure Al and Al-Mg syntactic foam composites containing glass cenospheres, Compos. Part A Appl. Sci. Manuf. 87 (2016) 194–202. doi:10.1016/j.compositesa.2016.05.001
[33] L. P. Zhang, Y. Y. Zhao, Mechanical response of Al matrix syntactic foams produced by pressure infiltration casting, J. Compos. Mater. 41 (2007) 2105–2117. doi:10.1177/0021998307074132
[34] I. N. Orbulov, J. Dobránszky, Producing metal matrix syntactic foams by pressure infiltration, Period. Polytech. Mech. Eng. 52 (2008) 35–42. doi:10.3311/pp.me.2008-1.06
[35] M. Taherishargh, I. V. Belova, G. E. Murch, T. Fiedler, Pumice/aluminium syntactic foam, Mater. Sci. Eng. A 635 (2015) 102–108. doi:10.1016/j.msea.2015.03.061
[36] R. A. Palmer, K. Gao, T. M. Doan, L. Green, G. Cavallaro, Pressure infiltrated syntactic foams – Process development and mechanical properties, Mater. Sci. Eng. A 464 (2007) 85–92. doi:10.1016/j.msea.2007.01.116
[37] M. Taherishargh, E. Linul, S. Broxtermann, T. Fiedler, The mechanical properties of expanded perlite-aluminium syntactic foam at elevated temperatures, J. Alloys Compd. 737 (2018) 590–596. doi:10.1016/j.jallcom.2017.12.083
[38] C. Qian, C. Liang, Z. He, W. Ji, Effect of layer thickness in layered aluminum matrix syntactic foam, Materials 12 (2019) 4172. doi:10.3390/ma12244172
[39] S. Sahu, M. Z. Ansari, D. P. Mondal, Microstructure and compressive deformation behavior of 2014 aluminium cenosphere syntactic foam made through stir casting technique, Mater. Today Proc. 25 (2020) 785–788. doi:10.1016/j.matpr.2019.09.019
[40] D. P. Mondal, M. D. Goel, V. Upadhyay, S. Das, M. Singh, A. K. Barnwal, Comparative study on microstructural characteristics and compression deformation behaviour of alumina and cenosphere reinforced aluminum syntactic foam made through stir casting technique, Trans. Indian Inst. Met. 71 (2018) 567–577. doi:10.1007/s12666-017-1211-x
[41] C. S. Chaitanya, R. N. Rao, Surface failure of syntactic foams in sliding contact, Mater. Today Proc. 15 (2019) 63–67. doi:10.1016/j.matpr.2019.05.025
[42] Y. M. Chordiy, M. D. Goel, Low velocity impact behavior of aluminum cenosphere syntactic foam, Mater. Today Proc. 18 (2019) 3741–3748. doi:10.1016/j.matpr.2019.07.309
[43] D. W. Rao, Y. W. Yang, Y. Huang, J. B. Sun, L.W. Pan, Z. L. Hu, Microstructure and compressive properties of aluminum matrix syntactic foams containing Al_2O_3 hollow particles, Kovove Mater. 58 (2020) 395–407. doi:10.4149/km.2020_6_396
[44] M. Taherishargh, I. V. Belova, G. E. Murch, T. Fiedler, Low-density expanded perlite-aluminium syntactic foam, Mater. Sci. Eng. A 604 (2014) 127–134. doi:10.1016/j.msea.2014.03.003
[45] N. Mahathaninwong, T. Plookphol, J. Wannasin, S. Wisutmethangoon, T6 heat treatment of rheocasting 7075 Al alloy, Mater. Sci. Eng. A 532 (2012) 91–99. doi:10.1016/j.msea.2011.10.068
[46] ISO 13314-2011, Mechanical Testing of Metals-Ductility Testing-Compression Test for Porous and Cellular Metals. International Organization for Standardization, Geneva.
[47] L. Licitra, D. D. Luong, O. M. Strbik, N. Gupta, Dynamic properties of alumina hollow particle filled aluminum alloy A356 matrix syntactic foams, Mater. Des. 66 (2015) 504–515. doi:10.1016/j.matdes.2014.03.041
[48] D. D. Luong, O. M. Strbik, V. H. Hammond, N. Gupta, K. Cho, Development of high performance lightweight aluminum alloy/SiC hollow sphere syntactic foams and compressive characterization at quasi-static and high strain rates, J. Alloys Compd. 550 (2013) 412–422. doi:10.1016/j.jallcom.2012.10.171
[49] Y. Zhang, Y. Zhao, Hysteretic energy dissipation in aluminium matrix syntactic foam under intermittent cyclic compression, Materialia 6 (2019) 100286. doi:10.1016/j.mtla.2019.100286
[50] ASM Handbook, vol. 4: Heat Treating, ASM Handbook Committee, pp. 841–879.
[51] Z. Y. Dou, L. T. Jiang, G. H. Wu, Q. Zhang, Z. Y. Xiu, G. Q. Chen, High strain rate compression of cenosphere-pure aluminum syntactic foams, Scr. Mater. 57 (2007) 945–948. doi:10.1016/j.scriptamat.2007.07.024
[52] T. Fiedler, K. Al-Sahlani, P. A. Linul, E. Linul, Mechanical properties of A356 and ZA27 metallic syntactic foams at cryogenic temperature, Journal of Alloys and Compounds 813 (2020) 152181. doi:10.1016/j.jallcom.2019.152181